ELSEVIER

International Journal of Solids and Structures 41 (2004) 4939–4958

INTERNATIONAL JOURNAL OF SOLIDS and STRUCTURES

www.elsevier.com/locate/ijsolstr

Deformation of solder joint under current stressing and numerical simulation—I

Hua Ye *, Cemal Basaran, Douglas C. Hopkins

UB Electronic Packaging Laboratory, Civil Engineering Department, 212 Ketter Hall, North Campus, SUNY at Buffalo, NY 14260, USA

Received 9 September 2003; received in revised form 28 March 2004
Available online 10 May 2004

Abstract

In this paper, Moiré interferometry technique is used to measure the in situ displacement evolution of lead-free solder joint under electric current stressing. Large deformation was observed in solder joint under high density (10^4 A/cm^2) current stressing. The deformation was found to be due to electromigration in the solder joint. An electromigration constitutive model is applied to simulate deformation of lead-free solder joint under current stressing. The simulation predicts reasonably close displacements results to Moiré interferometry experimental results in both spatial distribution and time history evolution, which indicates that the electromigration model is reasonably good for predicting the mechanical behavior of lead-free solder alloy under electric current stressing. This is the first part of the papers reporting the deformation of solder joint under current stressing. More experimental results are reported in the second paper.

Keywords: Electromigration; Moiré interferometry; Solder joint; Modeling

1. Introduction

Electromigration in solder joints under high direct current density is known as a reliability concern for the future high density microelectronic packaging and power electronic packaging (Lee et al., 2001; Lee and Tu, 2001; Ye et al., 2002a,b,c; Ye et al., 2003a,c). The trend in flip-chip and ball grid array (BGA) packaging to increase I/O count drives the interconnecting solder joints to be smaller in size and, thus, carry higher current density. The current density will increase further as chip voltage decrease and absolute current levels increase. The same trend in current density in interconnecting solder joints is also occurring in flip-chip power semiconductors and evolving system-on-package power processor (Liu et al., 1999, 2000; Liu and Lu, 2001; Paulasto-Krockel and Hauck, 2001). A physical limit to increasing current density in both microelectronics and power electronics is electromigration in solder joints.

* Corresponding author. Tel.: +1-716-645-2114x2429; fax: +1-716-645-3733.
E-mail addresses: cjb@eng.buffalo.edu, huaye@acsu.buffalo.edu (H. Ye).

0020-7683/$ - see front matter © 2004 Elsevier Ltd. All rights reserved.
doi:10.1016/j.ijsolstr.2004.04.002

In this paper, the deformation of lead-free solder joint under high density current stressing is measured with Moiré interferometry technique. Lead-free solder was used to fabricate the test module. The lead-free solder alloy used in the Moiré Interferometry experiment is Sn95.5/Ag4/Cu0.5. The melting point of this lead-free solder alloy is 218 °C. Sn/Ag/Cu alloy has better reliability properties than Sn/Ag alloy (Seelig and Suraski, 2001). Therefore, Sn95.5/Ag4/Cu0.5 solder alloy is used in our experiments as the candidate for lead-free solder alloy. Due to the improved thermal management in the experiments, very high current density (10^4 A/cm^2) was applied to the solder joint without much heat generation.

An electromigration constitutive model is presented and applied to simulate the stress evolution in the passivated metal line under current stressing in an early paper (Ye et al., 2003b). In this paper, the model is extended to the electromigration in lead-free solder joint. A numerical simulation of the deformation evolution is performed and compared with the experimental results.

2. Test sample and fixture schemes

In a previous Moiré interferometry experiment (Ye et al., in press) it was found that much heat was generated at the contact interface of test fixture and the BGA module during current stressing. Normally, the contact resistance can be reduced if greater clamping force is applied. However, the "Z" shape of test module used in the previous test makes it difficult to apply high clamping pressure without creating large shear deformation in the solder joint. This is because that the height of the solder joint cannot be controlled to be absolutely precise during solder reflow. In order to solve this problem, improved schemes of test module and fixture are introduced in the following experiment.

Fig. 1 shows the improved scheme of the test BGA module. The fabrication of BGA module follows the same procedure as described in our previous paper (Ye et al., in press). But instead of sectioning the test module into the "Z" shape, the test module is sectioned into the shape as shown in Fig. 1. The thickness of the copper plate is increased to 0.6 mm. A dielectric nylon spacer is glued between the upper and lower copper plates with epoxy to make the module less susceptible to mechanical deformation when higher clamping pressure is applied. There are two solder joints on the test module. A gap is sectioned in the lower copper plate in order to force the solder joints to carry the electric current (Fig. 1). One solder joint is purposely made much bigger than the other. Therefore, electromigration is restricted in the smaller solder joint (it is further carefully polished down to a very thin thickness), which carries much higher current density. Moiré interferometry experiment is only done on the smaller solder joint. The improved scheme of test fixture is shown in Fig. 2.

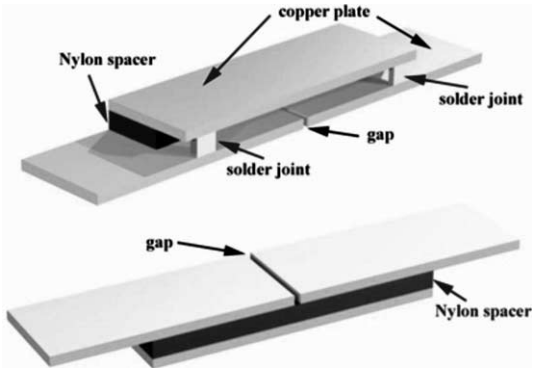

Fig. 1. New scheme of the test BGA module.

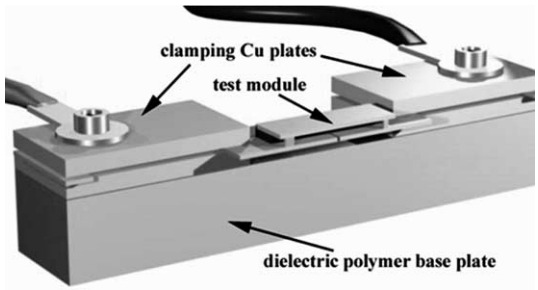

Fig. 2. New scheme of the test vehicle fixture.

Copper plates are used to clamp the test module in order to reduce electric contact resistance. In this improved schemes of test module and fixture, much higher clamping pressure can be applied without introduce large deformation in the solder joint. It is shown in the following experiment that the electric contact resistance is greatly reduced with these improved measures.

3. Moiré interferometry experiment on lead-free solder joint

The Moiré interferometry technique is explained extensively by Post et al. (1994). The major advantage of Moiré Interferometry is its high sensitivity, high resolution, and the whole field view of deformation distribution of the specimen surface. Briefly, the optical diffraction grating is replicated on the specimen surface. The specimen grating diffracts the incident two coherent laser beams with certain incident angle, and in the direction normal to the specimen surface, two strong diffracted beams are obtained. When the specimen surface deforms, the optical diffraction grating deforms with the specimen, and the two diffracted beams in the normal direction generate feature interferometry pattern that represents the in-plane displacement distribution. This scheme applies to both horizontal and vertical direction, so that deformation in the two perpendicular directions can be obtained. The feature fringe pattern generated by the vertical two beams (V field fringes) represents the relative vertical deformation field, and the fringe pattern generated by the horizontal two beams (U field fringes) represents the relative horizontal deformation field (Zhao et al., 2000). The Moiré fringes in the U and V fields represent isopleths of relative horizontal and vertical displacement, respectively.

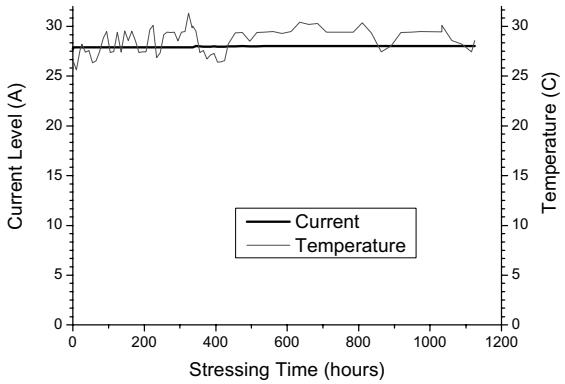

Fig. 3. Profile of applied current and measured temperature history for M-Pbfree-3.

The set-up of the stressing circuitry in our previous paper (Ye et al., in press). In this experiment, we managed to reduce the cross-section of test solder joint in order to achieve high electric current density. The height of the solder joint is 1.5 mm and the width is reduced to 1 mm. The thickness of the solder joint is polished down to about 0.25 mm. In the experiment, 28 A of current was applied and a current density

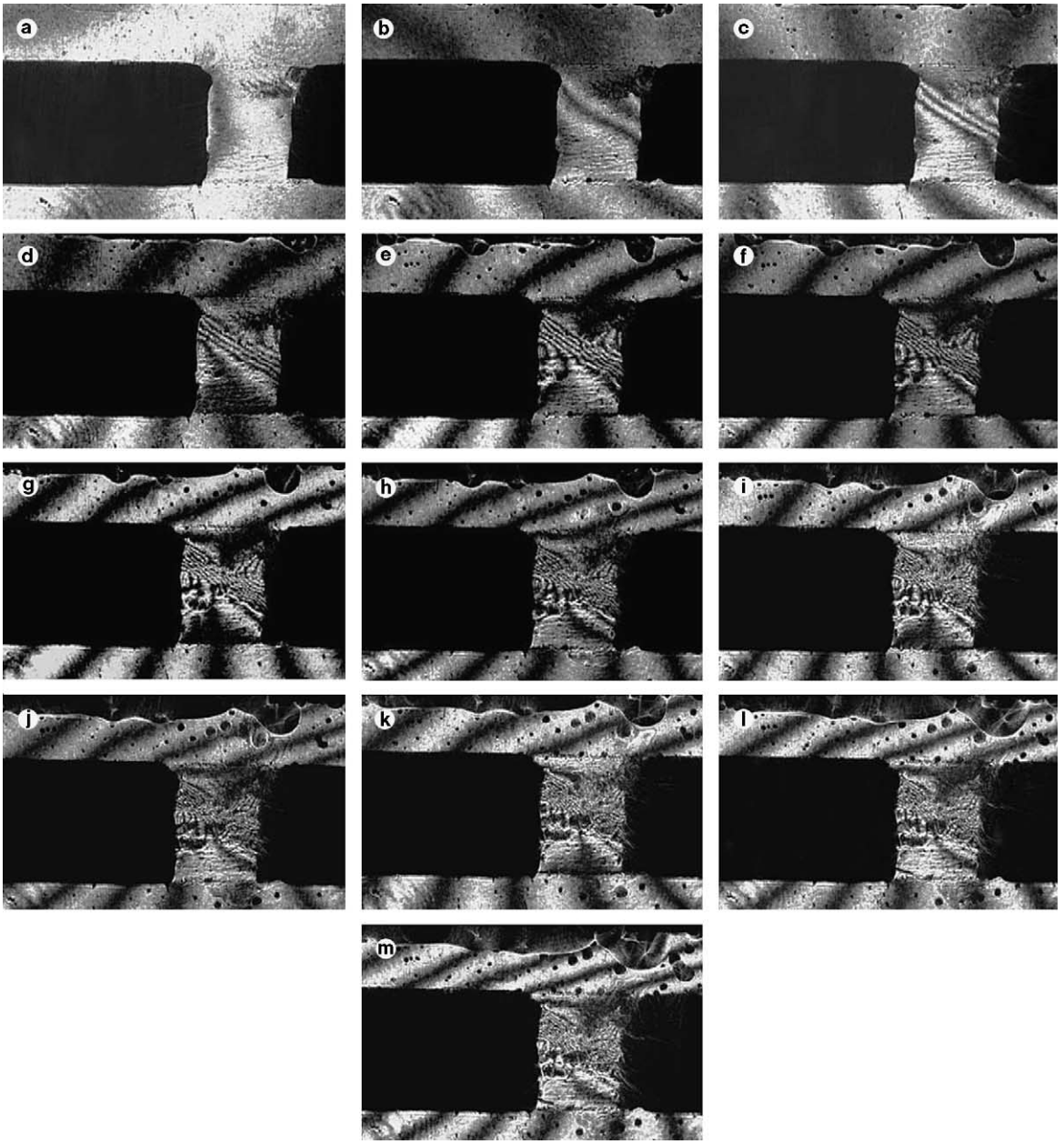

Fig. 4. U field fringe evolution: (a) initial, (b) 125 h, (c) 189 h, (d) 292 h, (e) 390 h, (f) 482 h, (g) 556 h, (h) 645 h, (i) 765 h, (j) 839 h, (k) 935 h, (l) 1033 h, (m) 1125 h.

around 1.12×10^4 A/cm^2 was achieved in the solder joint. The current flow direction is controlled to be from upper copper plate downward to lower copper plate in the test solder joint. The temperature was kept almost constant at 29 °C as shown in Fig. 3. There were some fluctuations of temperature (within 4 °C) during current stressing (considering this experiment took over a month, the fluctuation is reasonable).

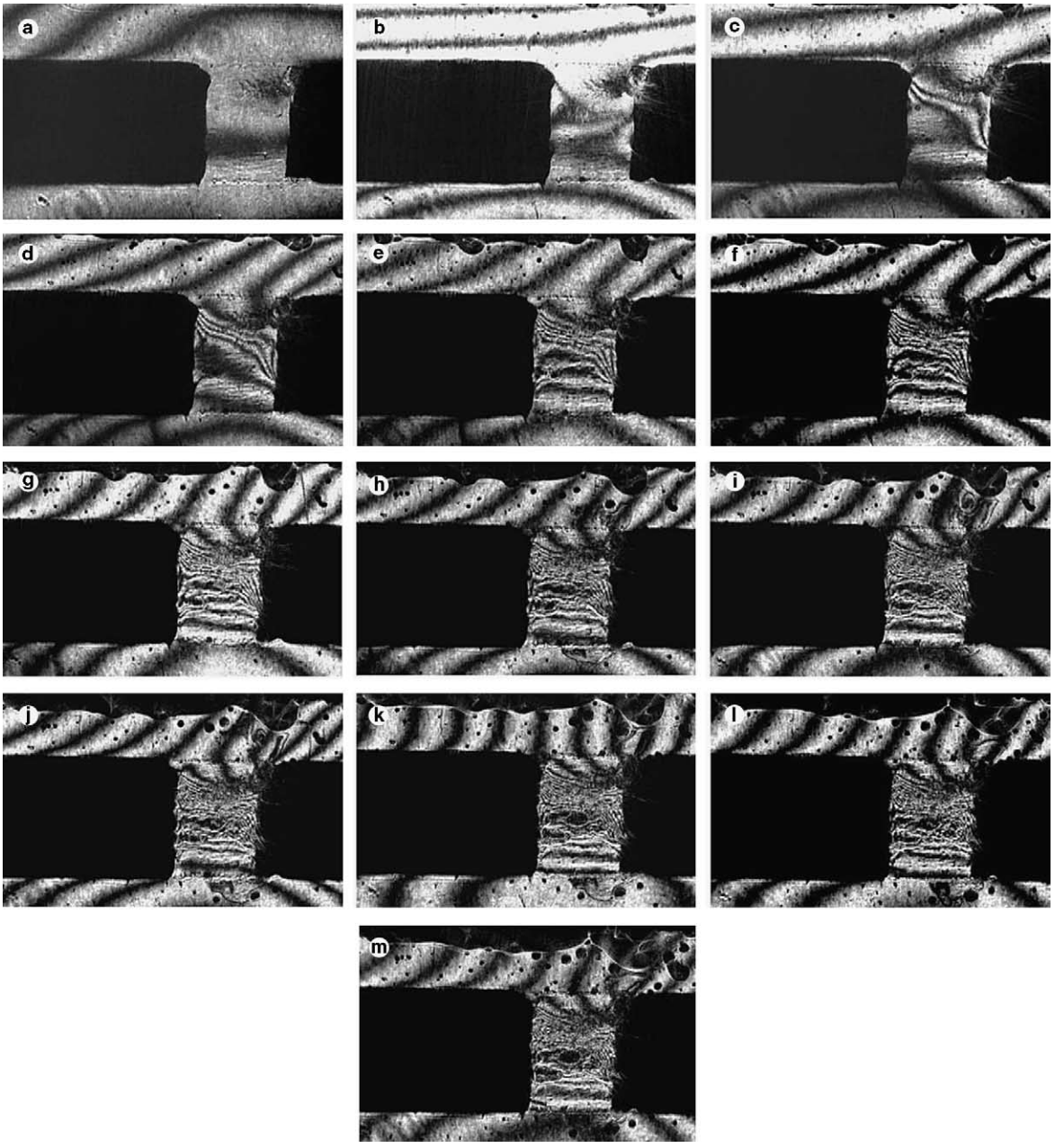

Fig. 5. V field fringe evolution: (a) initial, (b) 125 h, (c) 189 h, (d) 292 h, (e) 390 h, (f) 482 h, (g) 556 h, (h) 645 h, (i) 765 h, (j) 839 h, (k) 935 h, (l) 1033 h, (m) 1125 h.

Temperature measurement with a thermocouple confirmed that the clamping interface did not have a higher temperature than that atop the copper plate of the test module. The effectiveness of the improved test module and fixture design is clearly demonstrated by the fact that the temperature increase is much lower than that in the preliminary experiment (Ye et al., in press) when much higher electric current is applied.

The Moiré fringe evolution of the solder joint is shown in Figs. 4 and 5 for U and V fields, respectively. Both U and V fields developed a lot of fringes during the course of current stressing. The U field fringes were predominantly in the vertical direction with concentrations on both vertical edges; indicating that large normal deformation was developed in horizontal direction. The horizontal normal deformation was not uniform along the height of the solder joint. Only a couple of horizontal fringes were developed in the U field at the early stage of current stressing, which indicates that there was a little shear deformation developed due to thermal stressing (despite of better thermal management, there was still a 5 °C temperature increase during current stressing). The V field fringes were predominantly in the horizontal direction indicating large normal deformation in vertical direction. The evolutions of fringes in both fields were observed to be steady after 1000 h of current stressing; indicating the deformation of solder joint under electric current stressing reaches steady state after 1000 h of stressing.

The dense fringes observed in the solder joint is fundamentally different in several ways from those reported in our previous experiment (Ye et al., in press). First, the U field fringes were predominantly in horizontal direction and V field fringes were predominantly in vertical direction in the previous experiment, which indicates that shear deformation was dominant in the solder joint; whereas, there was only a very little shear deformation in this experiment and normal deformations in both horizontal and vertical direction were dominant. Second, there was large temperature increase in the previous experiment (a 15 °C increase atop of copper plate and a 35 °C increase near the clamping interface), where the thermal expansion of the copper plates contributed to the observed shear deformation in the solder joint, which was verified by an FEM simulation (Ye et al., in press). On the other hand, the temperature increase in this experiment was much lower and uniform across the whole test module. And the temperature was kept near constant for the rest hundreds of hours of current stressing. Therefore, thermal deformation cannot account for subsequent development of normal deformation during those hundreds of hours of current stressing. Third, the fringe development in the previous experiment took only hours if not minutes, which is the time for heat to transfer; but the development of fringes in this experiment took hundreds of hours to reach steady state. Such a long development time can only be explained by the coupled mechanical–diffusional electromigration process. Based upon the above analysis, it is clear that the deformation fringes we observed in this experiment are mostly due to current stressing (electromigration).

4. Irreversible deformations in solder joint after turning current off

In the current stressing experiment, the solder joints were stressed under high current density for a total of 1500 h. The deformation in the solder joint became unchanged after 1000 h of current stressing as shown in the previous section. We kept recording the deformation fringes after the turning the electric current off.

Figs. 6 and 7 show the U field and V field fields fringes in the solder joint after 1500 h of current stressing and 72 h after the current was turned off. Although the fringes in the solder joint became less clear after 1500 h of current stressing due to the degradation of diffraction grating, there were little changes in both U and V field fringes after the current was turned off for 3 days. This indicates that the deformations created by high current density are irreversible. However, these irreversible deformations are not the same as the plastic deformation. Plastic deformations are created by the high deviatoric (shear) stresses and correspond to the motion of large numbers of dislocations. The deformation created by electromigration is due to the re-arrangement of vacancies and atoms in the material as well as vacancy generations and annihilation due

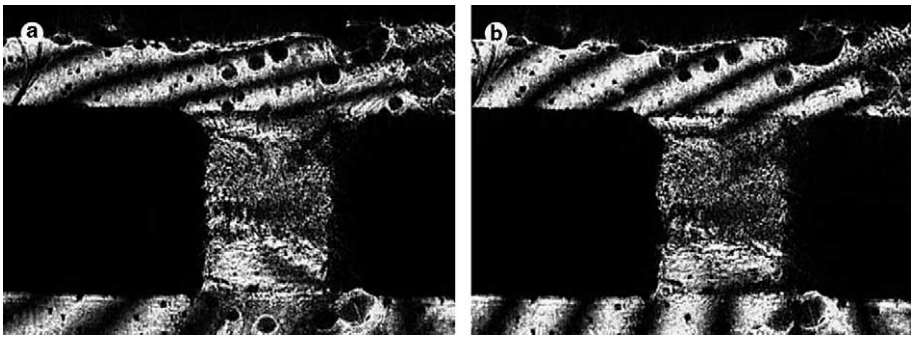

Fig. 6. U field fringe of module M-Pbfree-3 (a) 1500 h of current stressing, (b) 72 h after the current was turned off.

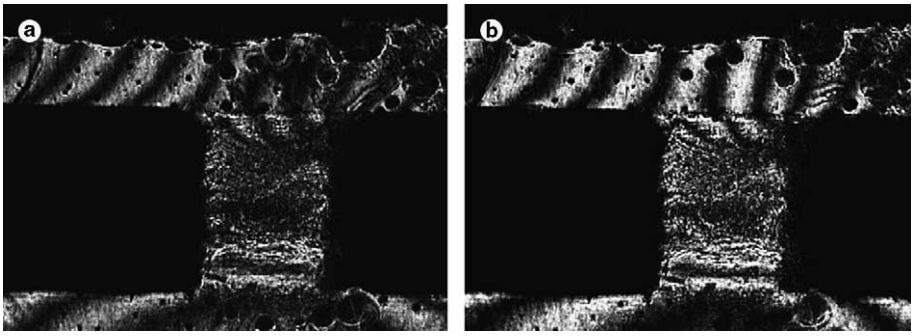

Fig. 7. V field fringe of module M-Pbfree-3 (a) 1500 h of current stressing, (b) 72 h after the current was turned off.

to diffusion and correspond to the local volumetric deformations. However, as demonstrated in the numerical simulations, local volumetric deformations due to electromigration give rise to high level stresses that exceed the yield stress of the solder alloy; these high deviatoric stresses may create plastic deformations. Therefore, the irreversible deformations we observed in the experiments are the combination of electromigration deformations and plastic deformations.

5. Numerical simulation of deformation of solder joint under current stressing

The electromigration is viewed as a coupled diffusion–mechanical process. The electron flow assisted vacancy diffusion process gives rise to local volumetric strain in the conducting solder alloy. Under the mechanical boundary constrains, the local volumetric strain due to diffusion results in stress build-up within the structure. If the spherical stress state within the conducting solder is changed or there is spherical stress gradient created, the stress state will in turn affect the vacancy flux or vacancy generation rate in the diffusion process. This coupled process is described by the following PDE system.

The vacancy diffusion equation of electromigration (Kirchheim, 1992):

$$\frac{\partial C_{\mathrm{v}}}{\partial t} = -\vec{\nabla} \cdot \vec{q} + G \tag{1}$$

$$\text{and} \quad \vec{q} = -D_{\mathrm{v}}\left[\vec{\nabla}C_{\mathrm{v}} + \frac{C_{\mathrm{v}}Z^{*}e}{kT}(-\rho\vec{j}) - \frac{C_{\mathrm{v}}}{kT}(-f\Omega)\vec{\nabla}\sigma\right]$$

combined, these two equations become

$$\frac{\partial C_{\mathrm{v}}}{\partial t} = D_{\mathrm{v}}\left[\nabla^{2}C_{\mathrm{v}} - \frac{Z^{*}e\rho}{kT}\vec{\nabla}\cdot(C_{\mathrm{v}}\vec{j}) + \frac{f\Omega}{kT}\vec{\nabla}\cdot(C_{\mathrm{v}}\vec{\nabla}\sigma)\right] + G \tag{2}$$

The volumetric strain due to vacancy diffusion (Sarychev and Zhinikov, 1999):

$$\dot{\varepsilon}_{ij}^{\mathrm{elec}} = \dot{\varepsilon}_{ij}^{\mathrm{m}} + \dot{\varepsilon}_{ij}^{\mathrm{g}} = \frac{\Omega}{3}[f\vec{\nabla}\cdot\vec{q} + (1-f)G]\delta_{ij} \tag{3}$$

The total strain in the solder alloy:

$$\varepsilon_{ij}^{\mathrm{total}} = \varepsilon_{ij}^{\mathrm{mech}} + \varepsilon_{ij}^{\mathrm{therm}} + \varepsilon_{ij}^{\mathrm{elec}} \tag{4}$$

And the quasi-static mechanical equilibrium equation for a 2-D problem:

$$\frac{\partial\sigma_{x}}{\partial x} + \frac{\partial\tau_{xy}}{\partial y} = 0 \tag{5}$$

$$\frac{\partial\tau_{xy}}{\partial x} + \frac{\partial\sigma_{y}}{\partial y} = 0 \tag{6}$$

The coupled diffusion-mechanical process can be model by solving the PDE system of Eqs. (2), (3), (5) and (6) for a 2-D problems. Where, in these equations, C_{v} is vacancy concentration, D_{v} is vacancy diffusivity, $\vec{q}$ is vacancy flux vector, Z^{*} is vacancy effective charge number, e is electron charge, ρ is metal resistivity, $\vec{j}$ is current density vector, f is vacancy relaxation ratio, Ω is atomic volume, k is Boltzman's constant, T is absolute temperature, $\sigma = \mathrm{trace}(\sigma_{ij})/3$ is hydrostatic or spherical part of the stress tensor, $G = -\frac{C_{\mathrm{v}}-C_{\mathrm{ve}}}{\tau_{\mathrm{s}}}$ is vacancy generation rate (Sarychev and Zhinikov, 1999) $C_{\mathrm{ve}} = C_{\mathrm{v0}}\mathrm{e}^{\frac{(1-f)\Omega\sigma}{kT}}$ is thermodynamic equilibrium vacancy concentration, C_{v0} is equilibrium vacancy concentration in the absence of stress, τ_{s} is characteristic vacancy generation/annihilation time, $\dot{\varepsilon}_{ij}^{\mathrm{m}} = \frac{1}{3}f\Omega\vec{\nabla}\cdot\vec{q}\delta_{ij}$ is volumetric strain due to vacancy migration, $\dot{\varepsilon}_{ij}^{\mathrm{g}} = \frac{1}{3}(1-f)\Omega G\delta_{ij}$ is volumetric strain due to vacancy generation, δ_{ij} is the Kronecker's symbol, $\varepsilon_{ij}^{\mathrm{total}}$ is the total strain tensor, $\varepsilon_{ij}^{\mathrm{mech}}$ is the strain due to mechanical loading, $\varepsilon_{ij}^{\mathrm{therm}}$ is the strain due to thermal expansion, and $\varepsilon_{ij}^{\mathrm{elec}}$ is the volumetric strain due to electromigration. The detailed formulation of the electromigration model is reported in a previous paper (Ye et al., 2003b). In the following simulations, only elastic mechanical constitutive model is employed since the primary purpose of the simulation is to verify the electromigration constitutive model. But since no elastic mechanical stress-strain relationship is assumed in this model, more realistic mechanical constitutive model can be employed in this model in the future.

6. Model parameters for lead-free solder alloy

In order to numerically simulate the deformation of lead-free solder joint under electric current stressing, one needs to identify the material parameters to be used in the constitutive model. There was little work done on the diffusion properties of lead-free solder alloy; but there are some diffusion and electromigration research work done on pure tin. Since the lead-free solder alloy used in this experiment contains 95.5% of tin, the material properties of tin are taken in the numerical simulation as a first order approximation.

6.1. Equilibrium vacancy concentration

The atomic volume, Ω, of tin is 16.3 cm^3/mol or 2.71×10^{-23} cm^3/atom. The atomic concentration, C_a, of tin is 3.69×10^{22}/cm^3 The equilibrium vacancy concentration at a stress-free state is reported as $C_{v0}/C_a = 3\times10^{-5}$ by Balzer and Sigvaldason (1979), or $C_{v0} = 1.11\times10^{18}$/cm^3.

6.2. Vacancy diffusivity

Some researches have been done on the diffusion and electromigration experiments of pure tin. Lange and Bergner (1962) measured the self-diffusion along grain boundaries in polycrystalline Sn (99.99%) between 40 and 115 °C. Sun and Ohring (1976) developed a tracer-scanning technique to study self-diffusion and electromigration in evaporated thin Sn films at 142–213 °C. Singh and Ohring (1984) conducted the self-diffusion and electromigration experiment in evaporated thin Sn films at −50 to +198 °C. Their measurements of grain boundary diffusivity in pure tin are shown in Fig. 8. The Lange and Bergner measurement agrees closely with that of Singh and Ohring's.

The grain boundary diffusivity given by Singh and Ohring (1984) by assuming a grain boundary width of 0.5 nm is:

$$D_{gb} = (4.9^{+15.6}_{-3.7})\exp[-(11,700\pm840\ \text{cal/mol})/RT]\ \text{cm}^2/\text{s} \tag{7}$$

where $R = 8.3145$ J/mol $= 1.987$ cal/mol, is gas constant, T is absolute temperature. In this simulation, grain boundary diffusion is assumed to be the main diffusion mechanism in electromigration. By assuming an average grain size of $d = 300$ nm (Singh and Ohring, 1984) the effective atomic diffusivity is thus:

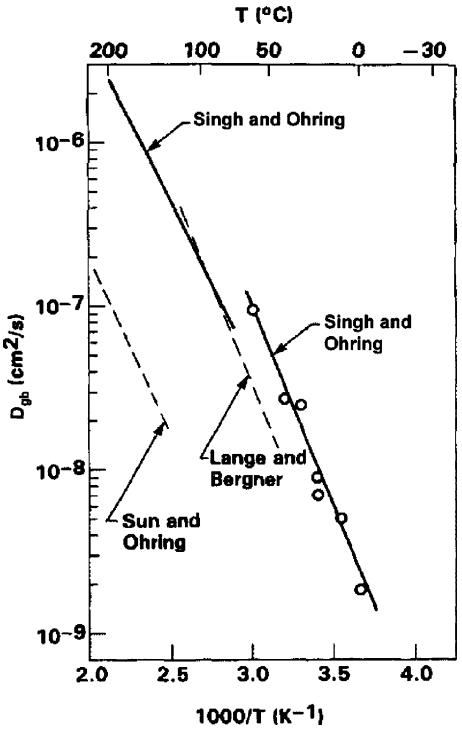

Fig. 8. Summery of D_{gb} values in Sn (after Singh and Ohring, 1984).

$$D_a = \frac{\delta}{d} D_{gb} = \frac{0.5\ \text{nm}}{300\ \text{nm}} \times 4.9 \times \exp(-11,700\ \text{cal}/RT])\ \text{cm}^2/\text{s} \tag{8}$$

At 303 K (30 °C), D_a is calculated to be 2.97×10^{-11} cm^2/s. The vacancy diffusivity is calculated from the relation (Clement and Thompson, 1995) $D_a C_a = D_v C_v$, at the stress-free state. By assuming $C_{v0}/C_a = 3 \times 10^{-5}$ (Balzer and Sigvaldason, 1979) $D_v = D_a/(3 \times 10^{-5}) = 1 \times 10^{-6}$ cm^2/s is derived and used in the following simulations.

6.3. Effective charge number Z^*

Lodding (1962) and Kuz'menko (1962) reported the effective charge number Z^* values of pure tin ranging from −80 to −160. Sun and Ohring reported similar values (Sun and Ohring, 1976). However, Khosla and Huntington (1975) reported effective charge number ranging from −10 to −16 in single-crystalline Sn and −12 in polycrystalline at temperature in the vicinity of 200 °C. Singh and Ohring found that the effective charge number of Sn is dependent on temperature, and their reported values are a little bit smaller than that by Khosla & Huntington. Sorbello (1973) developed an electromigration theory, which is based on the pseudopotential calculation of driving forces for atomic migration in metals in the presence of electric current, and predicted effective charge number of Sn to be −10 at 185 °C. Sorbello's theory favors the experimental results from Khosla and Huntington and Singh and Ohring. The effective charge number values vs. temperature from aforementioned references are plotted in Fig. 9.

The effective charge number of lead-free solder is chosen as $Z^* = -20$ at 30 °C (measured stressing temperature) based on these references. This negative effective charge number is for the atoms in the solder, indicating the atoms are actually migrating in the opposite direction of electric current. Since the vacancy migrates in the opposite direction of the moving atom, the effective charge number for the vacancy is positive. Therefore, in the simulation the effective charge number of vacancy is taken as $Z^* = 20$.

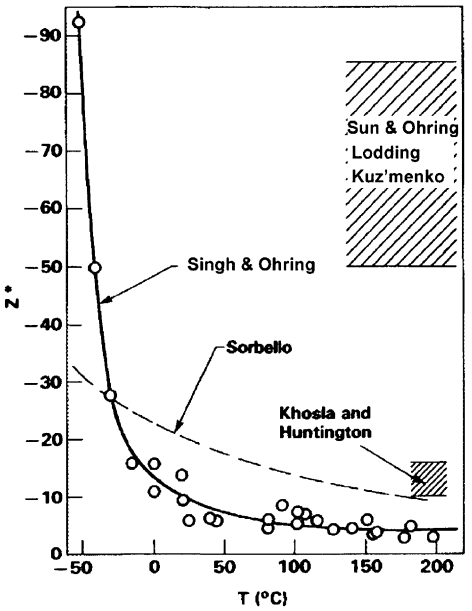

Fig. 9. Effective charge number in tin vs. temperature (after Singh and Ohring, 1984).

6.4. Other simulation parameters for lead-free solder alloy

$T = 303$ K, temperature (assumed as uniformly distributed in the solder joint). $K = 8.62 \times 10^{-5}$ eV/K $= 1.38 \times 10^{-23}$ J/K, Boltzman's constant; $\tau_s = 1.8 \times 10^{-3}$ s, vacancy relaxation time (Sarychev and Zhinikov, 1999); $f = 0.6$, average vacancy relaxation ratio (Sarychev and Zhinikov, 1999); $\rho = 1.15 \times 10^{-5}$ Ωcm, electrical resistivity; $E = 41.4$ GPa $= 4.14 \times 10^6$ N/cm^2 Young's modulus; $n = 0.33$, Poisson's ratio.

The single crystal Sn is a highly anisotropic material. However, the solder alloy we used, which consists of 95.5% of Sn, has very small grain size. The SnAg3.5 solder has a lamella morphology with a phase size of 2–3 μm (Jang et al., 2001). The actual grain size is smaller. Therefore, in a solder joint we tested, which is 1000 μm × 1500 μm with a thickness at least 250 μm, the number of grains is very large. Based on the large number of grains contained in a solder joint, the use of a single modulus and resistivity is justified.

7. FEM simulation model and boundary conditions

FlexPDE is used as the finite element code in the simulation (FlexPDE, 2002). A brief description of this software can be found in our previous paper (Ye et al., 2003b). A two-dimensional simulation model is employed in order to simplify the computational complexity. Fig. 10 shows the simulation model and the displacement boundary conditions. This 2-D model is the simplification of the real test structure as shown in Fig. 2. Both the horizontal and vertical displacements at far end of the lower copper plate are assumed to be fixed due to the clamping of the fixture. The horizontal and vertical displacements at far end of the upper copper plate are also assumed to be fixed due to the restriction from the embedded nylon spacer. The diffusion boundary condition is that vacancy fluxes on all the edges are zero (natural boundary condition).

Since the solder joint is polished to be a very thin film (0.2–0.3 mm average in thickness), plane stress assumption is applied to solder joint. One the other hand, the widths of the copper plates are over 40 times wider than the thickness of solder joint; therefore, plane strain assumption is applied to copper plates. The plane strain formulation for the elastic mechanical stress–strain electromigration model is derived in detail in our previous paper (Ye et al., 2003b).

8. Assumptions for copper plates

Since the copper plates have much larger cross-section than that of solder joint, electromigration is only expected in the solder joint. Therefore, the current density in the copper plate is assumed to be zero. The interface between the copper plate and solder joint is treated by assuming that the diffusivity of copper is much smaller than that of solder. This treatment is a simplification because the vacancy diffusion process on the copper–solder interfaces are not clearly understood. The volumetric strain due to current stressing is explicitly treated as zero in the copper plate to further reduce the computational complexity. The material properties of copper are as follows:

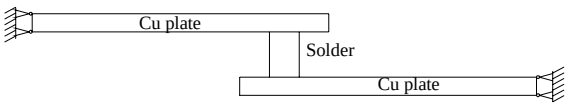

Fig. 10. FEM model and boundary conditions.

$E = 117$ GPa $= 1.17 \times 10^7$ N/cm^2, Young's modulus.
$n = 0.33$, Poisson's ratio.

9. Simulation results

The width of the solder joint is 1 mm and the height is 1.5 mm. The thickness is not uniform as shown in Fig. 11(a) and is considered in the simulation. The thinnest portion is a little less than 250 mm and it is gradually thicker near the solder–copper plate interfaces.

The variation of the thickness leads to non-uniformity of the current density in the solder joint. In the simulation, the thickness of solder joint is assumed to be a continuous function of position along the height of the solder joint:

$$W_{\text{thickness}} = 0.025 \times \left[1 + 2.5 \times \left(\frac{y - 0.05}{0.1}\right)^2\right] \tag{9}$$

where $W_{\text{thickness}}$ is the thickness of solder joint, y is the position along the height of the solder joint, the unit here is cm. The variation of thickness described by this function is shown in Fig. 11(b). Since two-dimensional simulation is employed, the variation of thickness cannot be directly introduced in the simulation model. In the simulation, the effect of thickness variation is considered by using a non-uniform stressing current density in the solder joint, where plane stress assumption is still taken. The current density in a 1 mm wide and 0.25 mm thick solder joint is 1.12×10^4 A/cm^2. The non-uniform current density along the height of the solder joint is therefore assumed in the simulation as:

$$j = 1.12 \times 10^4 \Big/ \left[1 + 2.5 \times \left(\frac{y - 0.05}{0.1}\right)^2\right] \ (\text{A/cm}^2) \tag{10}$$

where j is current density. The current density is assumed uniformly distributed along the width of the solder joint.

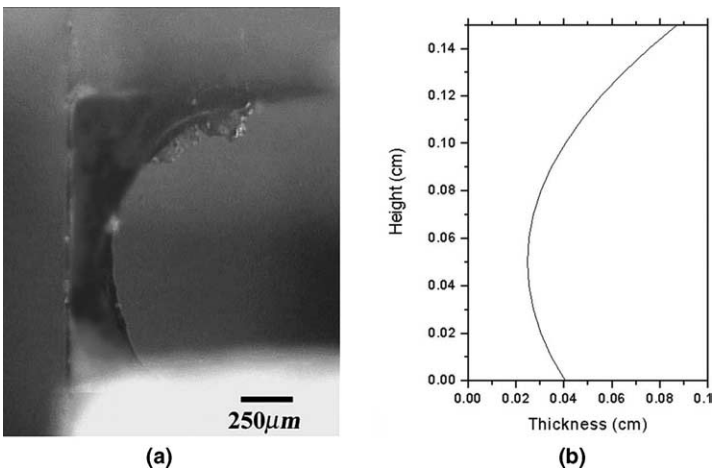

Fig. 11. Thickness of solder joint of M-Pbfree-3 (a) optical microscopic image, (b) thickness variation along the height of the solder joint used in the simulation.

Fig. 12 shows the FEM simulation mesh. The direction of current flow is from upper copper plate to lower copper plate. The following figures show length in cm, stress in N/cm^2, time in *second* unless otherwise noted.

Figs. 13 and 14 show the simulated distributions of horizontal and vertical displacements within the solder joint along side with the Moiré interferometry measurement after 600 h of current stressing. They clearly show that simulation results have caught the most important characteristics of the measured displacement fields.

The simulated distributions of both horizontal and vertical displacements resemble the distributions measured by experiment: there are large normal deformation developed in the horizontal direction but the horizontal normal deformations are not uniform along the both edges of the solder joint; there are also large normal deformation developed in the vertical direction. The simulation results are not exactly the same as the experiment measurements. But considering all the assumptions (solder diffusivity, effective charge number, thermal equilibrium vacancy concentration, and vacancy relaxation time, etc.) that were taken and many simplifications (the thickness variation of the solder joint, 2-D simplification of the 3-D structure, the treatments of copper plates and solder–copper interface, and elastic assumption of the mechanical constitutive model for lead-free solder alloy, etc.) of the simulation model, the simulation results are quit reasonable.

As shown in the experiment, the fringes measured in the solder joint gradually increased with stressing time and reached steady state after 1000 h of stressing. The simulation results show the similar trend. The maximum relative vertical displacement between the solder–copper interfaces (relative vertical displacement between points C and D in Fig. 14(b)) and maximum relative horizontal displacement between the two edges of the solder joint (relative horizontal displacement between points A and B in Fig. 13(b)) are chosen to compare their time history evolutions between the simulation results and experiment measurements. Fig. 15 shows the comparison of maximum relative vertical displacement between the two copper–solder

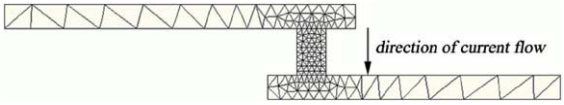

Fig. 12. FEM simulation mesh.

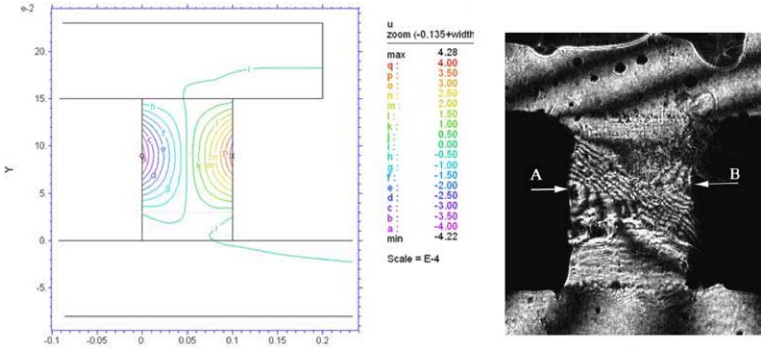

Fig. 13. (a) Simulated horizontal displacement after 600 h of current stressing. (b) U field fringe development after 605 h of current stressing.

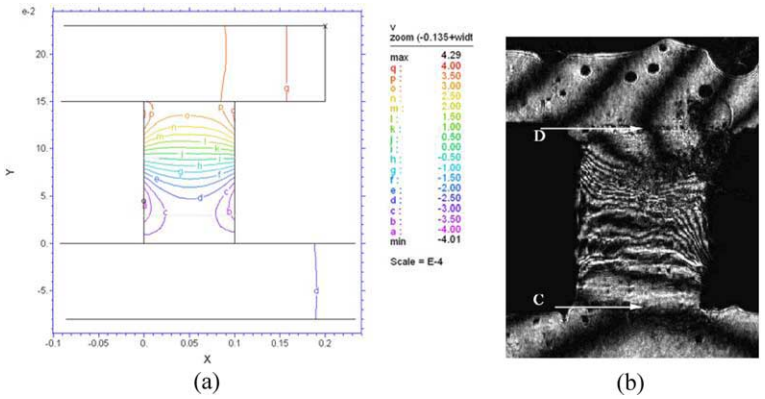

Fig. 14. (a) Simulated vertical displacement after 600 h of current stressing. (b) V field fringe development after 605 h of current stressing.

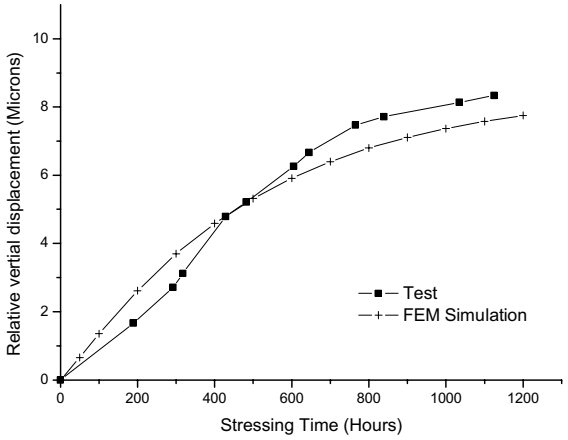

Fig. 15. Evolution of relative vertical displacement between lower and upper interface of solder joint and copper plates in M-Pbfree-3.

interfaces. The FEM simulation predicts higher than experimental measured values for the first 500 hundred h of current stressing and lower values after 500 h of stressing. The simulation indicates that the developing rate of relative vertical displacement decrease with stressing time; whereas, the experimental observation shows the largest increase rate of relative vertical displacement took place between 300 and 800 h of current stressing. Both simulation and experimental results show that the relative vertical displacement approached steady state after 1000 h of current stressing. Fig. 16 shows the evolution of maximum relative horizontal displacement between the two edges of the solder joint. The FEM simulation result is always higher than experimental result and they both approach steady state after 1000 h of current stressing. As shown in these two figures, the simulated time history evolution results closely match the experimental results although they are not identical. Therefore, both the spatial distribution and time history evolution of displacements confirm that the electromigration model used in this simulation is valid for lead-free solder alloy.

Fig. 17 shows the exaggerated deformed shape of the test module after 600 h of current stressing. The simulated spherical stress distribution within M-Pbfree-3 after 600 h of current stressing is shown in Fig. 18.

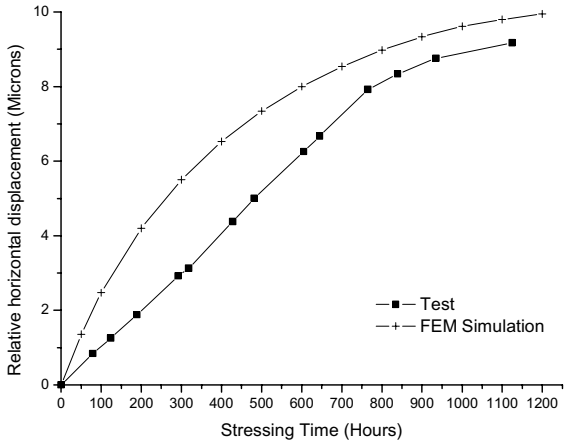

Fig. 16. Evolution of maximum relative horizontal displacement between the two edges of the solder joint in M-Pbfree-3.

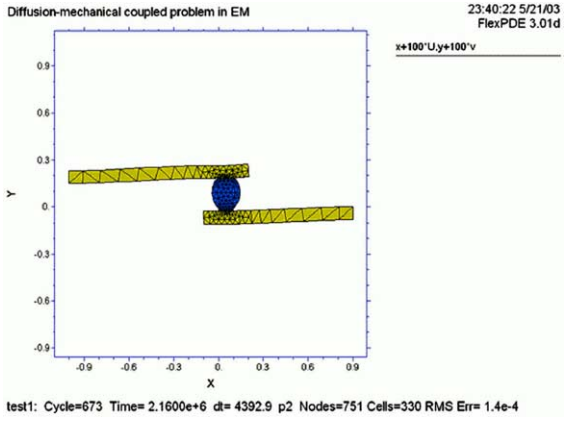

Fig. 17. Simulated deformation of M-Pbfree-3 after 600 h of current stressing.

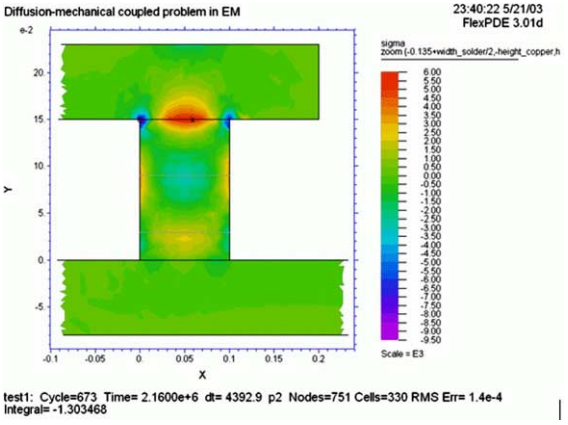

Fig. 18. Simulated spherical stress distribution in M-Pb-free-3 after 600 h of current stressing.

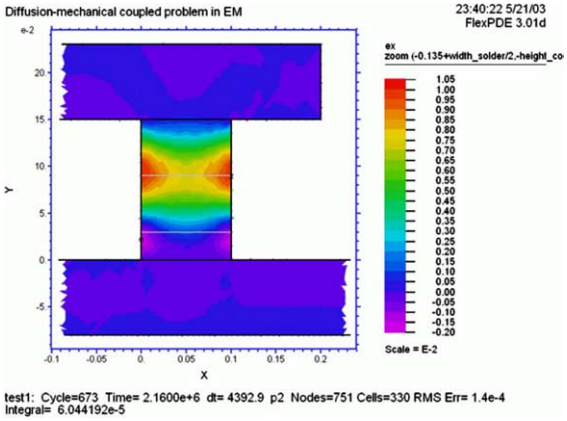

Fig. 19. Simulated normal strain ε_x distribution after 600 h of current stressing.

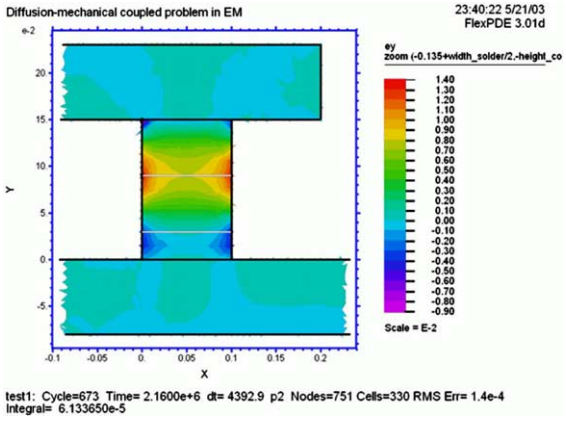

Fig. 20. Simulated normal strain ε_y distribution after 600 h of current stressing.

Both the maximum positive and negative spherical stresses occur on the interface between the upper copper plate and solder joint. The maximum spherical stress is on the order of 60 MPa. Figs. 19–21 show the distributions of normal and shear strains, ε_x, ε_y, and γ_{xy}, within the solder joint after 600 h of current stressing. The normal strains are found to be dominant and on the order of 1%. The shear strain is found highly localized within the solder joint and its maximum value is only on order of 0.4% which is much smaller than the maximum normal strains. The strains are found to be almost symmetric along the vertical center line. But these strains are non-symmetric along the horizontal center line. This is due to the non-uniform distribution of current density within the solder joint as assumed in Eq. (10). The distributions of normal and shear stresses, σ_x, σ_y, and τ_{xy}, within the solder joint after 600 h of current stressing are shown in Figs. 22–24. The maximum positive and negative normal stress, σ_x, is found to be on the interface of upper copper plate and solder joint and is on the order of 120 MPa. The maximum normal stress, σ_y, is found to be on the both edges of the solder joint and is on the order of 120 MPa. Like the shear strain, the shear stress is localized within the solder joint and its maximum value is on the order of 60 MPa. The symmetries of the stresses are similar to that of strains due to distribution of current density.

Despite of all the assumptions and simplifications employed in the simulation, the simulation predicts reasonably close displacements results to Moiré interferometry experimental results in both spatial distri-

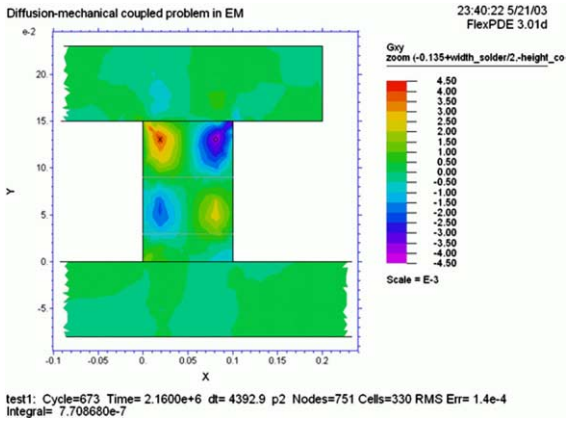

Fig. 21. Simulated shear strain γ_{xy} distribution after 600 h of current stressing.

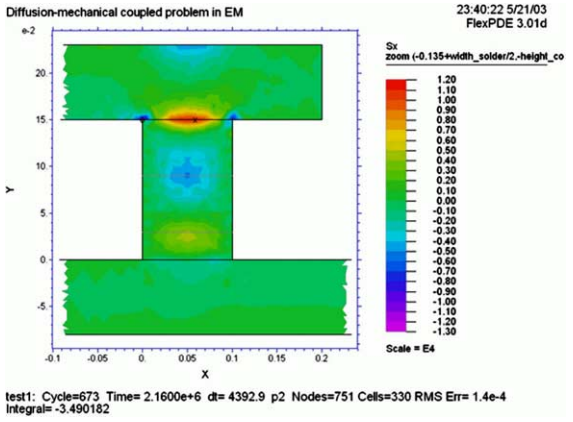

Fig. 22. Simulated normal stress σ_x distribution after 600 h of current stressing.

bution and time history evolution. This indicates that the electromigration model employed in this simulation is reasonably good for predicting the mechanical behavior of lead-free solder alloy under electric current stressing.

The FEM simulation predicts that both the horizontal and vertical displacement fields are symmetric with respect to the central vertical line of solder joint as shown in Figs. 13(a) and 14(a) during current stressing. But Figs. 13(b) and 14(b) show that the Moiré fringes in U and V fields are not perfectly symmetric to the central vertical line. The author thinks that the discrepancy comes from the thickness assumption of the solder joint. In the simulation, the variation of the thickness of the solder joint along its height is considered but the thickness along the width of solder joint at any height is assumed to be the same. This may not be the case. The non-uniformity of the thickness of the test solder joint along its width contributes to the non-symmetric observation of its Moiré fringes. Thermal expansion can also contribute to the non-symmetric observation of Moiré fringes, which is not considered in the simulation.

Another discrepancy between the simulation and experimental observation is the displacements time history evolution. As shown in Fig. 15, the simulation result of relative vertical displacement between lower and upper interfaces of solder joint and copper plates is higher than experimental observation during the

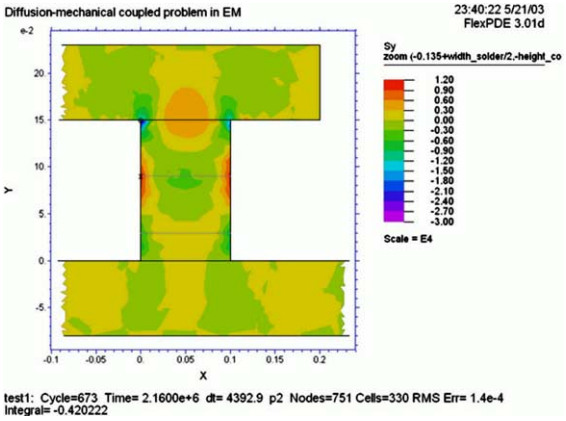

Fig. 23. Simulated normal stress σ_y distribution after 600 h of current stressing.

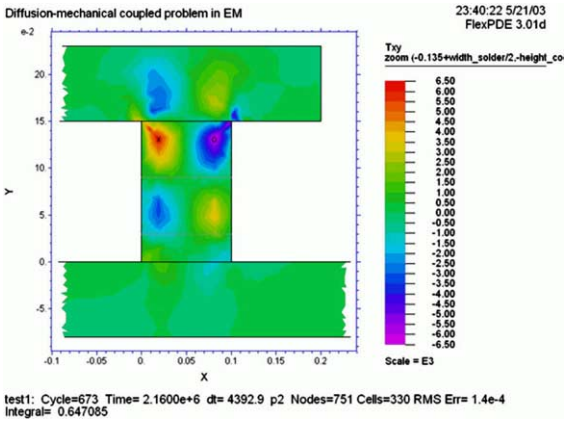

Fig. 24. Simulated shear stress τ_{xy} distribution after 600 h of current stressing.

first 500 h of current stressing and is lower than experimental observation after 500 h of current stressing. The simulation result of maximum relative horizontal displacement between the two edges of the solder joint is always higher than experimental observation as shown in Fig. 16. This discrepancy comes from the many assumptions that are taken in the simulation. All the diffusion and electromigration parameters of lead-free solder alloy, such as atomic diffusivity, vacancy diffusivity, thermal equilibrium vacancy concentration, and effective charge number, used in the simulation are taken from the diffusion and electromigration experiments of pure tin since there are few experiments in this area done for lead-free solder alloy. The simulation results should be improved when more diffusion and electromigration data are available for lead-free solder alloys.

10. Conclusions

In this paper, Moiré interferometry technique is used to measure the in situ displacement evolution of lead-free solder joint under electric current stressing. Large deformation was reported in solder joint under

high density (10^4 A/cm^2) current stressing. The deformation was found to be due to electromigration in the solder joint. The experimental observation reveals that the deformations created by high current density are irreversible. However, these irreversible deformations are not the same as the plastic deformation. Plastic deformations are created by the high deviatoric (shear) stresses and correspond to the motion of large numbers of dislocations. The deformation created by electromigration is due to the re-arrangement of vacancies and atoms in the material as well as vacancy generations and annihilation due to diffusion and correspond to the local volumetric deformations. However, as demonstrated in the numerical simulations, local volumetric deformations due to electromigration give rise to high level stresses that exceed the yield stress of the solder alloy; these high deviatoric stresses may create plastic deformations. Therefore, the irreversible deformations we observed in the experiments are the combination of electromigration deformations and plastic deformations. An electromigration constitutive model presented is applied to simulate deformation of lead-free solder joint under current stressing. Despite of all the assumptions and simplifications employed in the simulation, the simulation predicts reasonably close displacements results to Moiré interferometry experimental results in both spatial distribution and time history evolution. This indicates that the electromigration model employed in this simulation is reasonably good at predicting the mechanical behavior of lead-free solder alloy under electric current stressing.

References

Balzer, R., Sigvaldason, H., 1979. Equilibrium vacancy concentration measurements on tin single crystals. Physica Status Solidi B: Basic Research 92 (1), 143–147.

Clement, J.J., Thompson, C.V., 1995. Modeling electromigration-induced stress evolution in confined metal lines. Journal of Applied Physics 78 (2), 900–904.

Jang, J.W., De Silva, A.P., Lee, T.Y., Lin, J.K., Frear, D.R., 2001. Direct correlation between microstructure and mechanical tensile properties in Pb-free solders and eutectic SnPb solder for flip chip technology. Applied Physics Letters 79 (4), 482–484.

Khosla, A., Huntington, H.B., 1975. Electromigration in tin single crystals. Journal of Physics and Chemistry of Solids 36 (5), 395–399.

Kirchheim, R., 1992. Stress and electromigration in al-lines of integrated-circuits. Acta Metallurgica et Materialia 40 (2), 309–323.

Kuz'menko, P.P., 1962. Ukrainskii Fizicheskii Zhurnal (Russ. Ed.) 7, 117.

Lange, W., Bergner, D., 1962. Measurement of grain boundary self-diffusion in polycrystalline tin. Physica Status Solidi 2, 1410–1414.

Lee, T.Y., Tu, K.N., 2001. Electromigration of eutectic SnPb and SnAg3.8Cu0.7 flip chip solder bumps and under-bump metallization. Journal of Applied Physics 90 (9), 4502–4508.

Lee, T.Y., Tu, K.N., Kuo, S.M., Frear, D.R., 2001. Electromigration of eutectic SnPb solder interconnects for flip chip technology. Journal of Applied Physics 89 (6), 3189–3194.

Liu, X., Lu, G.-Q., 2001. D^2BGA chip-scale IGBT package. In: Proceedings of 16th Annual IEEE Applied Power Electronics Conference and Exposition, Anaheim, California.

Liu, X., Calata, J.N., Wang, J., Lu, G.-Q., 1999. The Packaging of Integrated Power Electronics Modules Using Flip-Chip Technology. CPES Seminar.

Liu, X., Jing, X., Lu, G.-Q.A., 2000. Comparative Study of Wire Bonding versus Solder Bumping of Power Semiconductor Devices. 2000 IEEE (IWIPP), Boston, MA.

Lodding, A., 1962. Current induced motion of lattice defects in indium metal. Journal of Physics and Chemistry of Solids 26 (1), 143–151.

Paulasto-Krockel, M., Hauck, T., 2001. Flip chip die attach development for multichip Mechatronics power packages. IEEE Transactions on Electronics Packaging Manufacturing 24 (4), 300–306.

Post, D., Han, B., Ifju, P., 1994. High Sensitivity Moire. Springer, New York.

Sarychev, M.E., Zhinikov, Y.V., 1999. General model for mechanical stress evolution during electromigration. Journal of Applied Physics 86 (6), 3068–3075.

Seelig, K., Suraski, D., 2001. Advanced materials considerations for lead-free electronics assembly. International Journal of Microcircuits and Electronic Packaging 24 (4), 366–378.

Singh, P., Ohring, M., 1984. Tracer study of diffusion and electromigration in thin tin films. Journal of Applied Physics 56 (4), 899–907.

Sorbello, R.S., 1973. Pseudopotential based theory of the driving forces for electromigration in metals. Journal of Physics and Chemistry of Solids 34 (6), 937–950.

Sun, P.H., Ohring, M., 1976. Tracer self-diffusion and electromigration in thin tin films. Journal of Applied Physics 47 (2), 478–485.

User Manual: FlexPDE. [3]. 2002. P.O. Box 4217, Antioch, CA 94531-4217, PDE Solutions Inc. http://www.PDESolutions.com.

Ye, H., Basaran, C., Hopkins, D., 2002a. Experiment study on reliability of solder joints under electrical stressing-nano-indentation, atomic flux measurement. In: Proceedings of 2002 International Conference on Advanced Packaging and Systems, Reno, Nevada.

Ye, H., Hopkins, D., Basaran, C., 2002b. Measurement and effects of high electrical current stress in solder joints. In: Proceedings of the 35th International Symposium on Microelectronics, Denver, Colorado, pp. 427–432.

Ye, H., Lin, M., Basaran, C., 2002c. Failure modes and FEM analysis of power electronic packaging. Finite Element in Analysis and Design 38 (7), 601–612.

Ye, H., Basaran, C., Hopkins, D., 2003a. Thermomigration in Pb–Sn solder joints under Joule heating during electric current stressing. Applied Physics Letters 82 (8), 1045–1047.

Ye, H., Basaran, C., Hopkins, D., 2003b. Numerical simulation of stress evolution during electromigration in IC interconnet lines. IEEE Transactions on Components and Packaging Technologies 26 (3), 673–681.

Ye, H., Basaran, C., Hopkins, D.C., 2003c. Damage mechanics of microelectronics solder joints under high current densities. International Journal of Solids and Structures 40 (15), 4021–4032.

Ye, H., Hopkins, D.C., Basaran, C., 2003. Measurement of high electrical current density effects in solder joints. Microelectronics Reliability 43 (12), 2021–2029.

Zhao, Y., Basaran, C., Cartwright, A., Dishongh, T., 2000. Thermomechanical behavior of micron scale solder joints under dynamic loads. Mechanics of Materials 32 (3), 161–173.